

# Discrete Element Simulation of Bending Beam Rheometer Tests for Asphalt Binder

Hui Yao<sup>1,3</sup>, Yu Liu<sup>2+</sup>, Zhanping You<sup>3</sup>, Liang Li<sup>1</sup> and Shu Wei Goh<sup>3</sup>

**Abstract:** This study presents a discrete element modeling approach to bending beam rheometer (BBR) tests for control and nanomaterial modified asphalt binders. In the discrete element model, a linear elastic contact model was used to simulate force displacement relations among adjacent elements, while a slip model and two bonding models were used to simulate the strength properties at each contact. The two bonding models include the contact bond model and parallel bond model, which were utilized simultaneously. In order to compute contributions of the two bonding models, a coefficient of  $\alpha$  was introduced. A compressive study found that discrete element simulation results were acceptable when  $\alpha$  was close to 1.0. Since asphalt materials exhibit time dependent behaviors and cannot be directly simulated with an elastic model, the time domain was represented by a few key time points that were simulated individually to account for the time dependency of asphalt materials. In order to obtain inputs for the discrete element model, BBR testing results of control and nanomaterial modified asphalt binder were fitted with the five-parameter Generalized Maxwell model, which represents the laboratory testing data well. A careful analysis of the discrete element simulation results indicates that 1) the discrete element model in this study can simulate a BBR test of asphalt binder, and 2) the stress and displacement distributions within the beam model can be virtualized and demonstrated.

**Key words:** *Bending Beam Rheometer (BBR); Discrete Element Method (DEM); Nanomaterials modified asphalt (NMA); Simulation.*

## Introduction

Asphalt is a viscoelastic building material of pavement, and its properties depend on its ambient temperature. Asphalt shows more elastic performance at low temperature and more viscous performance at high temperature [1-4]. Due to the repeated load of vehicles and cyclic nature of climate, asphalt pavement may appear distressed with thermal cracking, rutting, bleeding, fatigue cracking, scaling, etc. To prevent these distresses, the properties of asphalt and aggregates under different temperatures and loads should be known and improved [5-11].

According to the Superpave<sup>TM</sup> specification, thermal cracking is related to the low temperature performance of asphalt binder, and the Bending Beam Rheometer (BBR) test can be used to evaluate this performance [12-16]. BBR tests provide a measure of low temperature stiffness and the relaxation properties of asphalt binders. These parameters indicate an asphalt binder's ability to resist low temperature cracking. The basic BBR test is conducted on PAV aged asphalt binder samples. It uses the small asphalt binder beam, which is simply supported and immersed in a cold liquid bath. A load of 100 grams is applied to the center of the asphalt binder beam, and beam deflections are measured according to time. The beam dimension is 12.5 mm (width) by 6.25 mm (height) by 102 mm

(length). Stiffness is calculated based on the measured deflection and standard beam properties. Also, the measure of how asphalt binder relaxes the stress induced by load is carried out. The test method is similar to the three-point flexural beam test [13, 17].

According to recent research findings, the addition of Bentonite clay (BT) and organically modified bentonite (OBT) into base asphalt results in lower stiffness. In other words, the modified asphalt has better resistance in low temperature cracking [18]. In the literature [13, 19-22], the effect of adding wax S and wax PW to the base asphalt binder was studied through BBR tests at three temperatures. The results show that wax modification in asphalt binder increases the lower limit temperature of asphalt. It was observed that the presence of wax in the bitumen resulted in a hardening of the asphalt and asphalt mixture at low temperature [13, 19-22].

In addition, the effect of wax on asphalt and asphalt mixture performance depends on many factors, such as the chemical composition of asphalt and original source of wax. The bending beam test was applied to evaluate the low-temperature pavement performance of lightweight epoxy asphalt mixture (LEAM) on bascule bridges [23]. Test results show that LEAM has good resistance to moisture damage and low-temperature cracking. Obviously, nanotechnology is being developed rapidly as a novel technique in engineering. Due to the small sizes of nanoparticles, nanomaterials hold enormous potential for material application. Recently, nanoclay material was utilized to modify the base asphalt binder, and performance tests of the asphalt binder and mixture were carried out. The tests results show that the addition of nanoclay in the asphalt binder could improve the rutting and fatigue cracking resistance and decrease the moisture damage potential of asphalt mixture [5, 6, 24-26]. Therefore, the nanomaterial (micro-carbon nanotube) was selected for this study.

Finite element method (FEM) has been used to simulate bending

<sup>1</sup> School of Civil Engineering and Architecture, Central South University, Changsha 410075, China.

<sup>2</sup> Highway School, Chang'an University, Xi'an Shaanxi, 710064 China.

<sup>3</sup> Department of Civil and Environmental Engineering, Michigan Technological University, Houghton, Michigan 49931-1295, USA.

<sup>+</sup> Corresponding Author: E-mail yul@mtu.edu

Note: Submitted July 12, 2011; Revised December 10, 2011; Accepted December 19, 2011.

beam tests. The bending beam model was created, and the influence of bending beam thickness, width, depth, and position of the applied load on the beam displacement was investigated through a test simulation. The simulation results describe the geometric parameters effect and provide guidance on how to improve beam behaviors [12, 27, 28]. Meanwhile, the bending beam test can be done by the discrete element method (DEM), which can express the stress and displacement distributions in the bending beam.

Essentially, FEM is used to simulate the continuum type case, while the DEM is more suitable for modeling mixture internal discontinuities considering its component material properties considered. So far, the discrete element method has been used to simulate the special behaviors of asphalt mixture. Firstly, the effect of aggregate sphericity index, fractured faces, and orientation angles on the creep stiffness of hot mix asphalt (HMA) mixtures was investigated using a DEM simulation [29, 30]. Microstructure elastic and viscoelastic discrete element models were applied to simulate the creep compliance tests for asphalt mixtures, and the model results were very close to those measured in the laboratory. Also, the time-temperature superposition (TTS) principle was used to reduce computation time [4].

The creep behavior of asphalt mixture under uniaxial static loading was investigated by researchers, and Burger's model was applied to simulate the viscoelastic properties of asphalt mixture in DEM [30]. The research demonstrated that the creep compliance of secondary stage can be predicted accurately. However, there were errors in the primary stage [31]. The impact of asphalt binder stiffness values and volumetric fractions on the stiffness of asphalt sand mastic were evaluated, and the stiffness of fine and coarse sand mastics was predicted with a DEM micromechanical model [32]. Evidently, quite a lot of research efforts regarding asphalt mixture simulation were made through DEM modeling. Therefore, the DEM is used to simulate the behavior of asphalt binder in this study.

Additional studies are necessary for BBR tests of control and nano-modified binders and simulations to improve understanding between the laboratory tests and mechanical properties of the material. Discrete element method has been used as an important approach in the simulation of asphalt and asphalt mixture. As demonstrated in the subsequent sections, DEM was used to simulate BBR tests, and the results were compared with experimental results.

## Objectives and Scopes

The major objectives of this research are to 1) develop a discrete element model for simulating BBR tests of control and nano-modified asphalt binders, 2) calibrate the model parameters, 3) validate the newly developed model through comparing simulation results with BBR laboratory data, and 4) find the simulation model's stress and displacement distributions.

In order to achieve these objectives, nano-modified asphalt binder was studied through the discrete element simulation and laboratory tests of BBR. The BBR testing results were analyzed to provide model inputs and calibration or validation data. The discrete element simulation provided deep insight for an improved understanding of nano-modified asphalt materials and BBR tests. Additionally, viscoelastic models were used to analyze the BBR testing results.

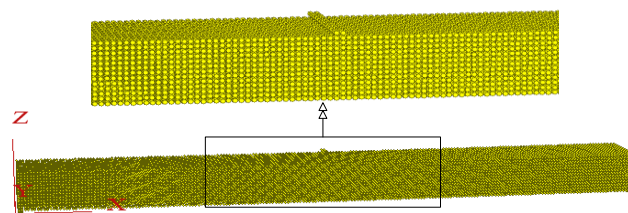


Fig. 1. Three-dimensional DEM Model for BBR Test.

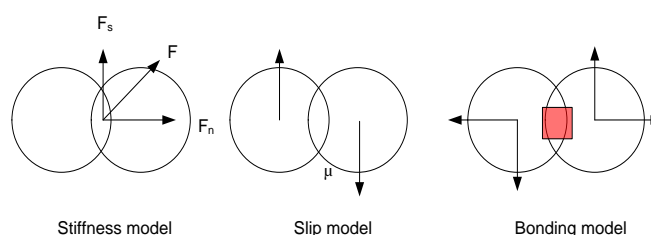


Fig. 2. Constitutive Models in DEM Model.

## Discrete Element Model

### Geometry

As shown in Fig. 1, the full size of BBR beams was simulated with a three dimensional model with dimensions of 12.5 mm width, 6.5 mm thickness, and 102 mm length. Considering the ball size in the DEM model, the thickness of the model was changed to 6.5 mm. Therefore, the overall size of model is 102 mm  $\times$  12.5 mm  $\times$  6.5 mm. A total of 66,300 balls with identical radiuses of 0.25 mm were used to build this three-dimensional digital beam. At the bottom of the two ends of the beam, two rows of balls were created to support the beam for bearing the applied loads. In the middle of the beam, two rows of balls were created for the load application.

### Mechanics

In the discrete element method, the materials' mechanical behaviors were simulated with constitutive models at contacts of discrete elements. Each constitutive model consists of three portions: a stiffness model, a slip model, and a bonding model [2, 3]. The stiffness model represents the force displacement relationship of two contacting elements, while the slip and bonding models simulate the strength properties of the contact. In this research, a linear elastic contact model was used as the stiffness model, which is defined through the normal and shear stiffness of the two contacting elements ( $K_n$ ,  $K_s$ ). The slip model was defined through the frictional coefficient ( $\mu$ ) at the contact point. The bonding model was defined by combining the contact bond model and parallel bond model. These constitutive models for material behaviors at each contact point are shown in Fig. 2. Details on these contact models can be found in relevant literature [33].

The DEM model of BBR tests was created, and the model verification work needed to be done. During this process of verification, the contact bond and parallel bond were considered, and coefficient  $\alpha$  was introduced to distribute the stiffness. A contact bond can be imaged as a set of elastic springs with the constant normal stiffness and shear stiffness acting at the contact

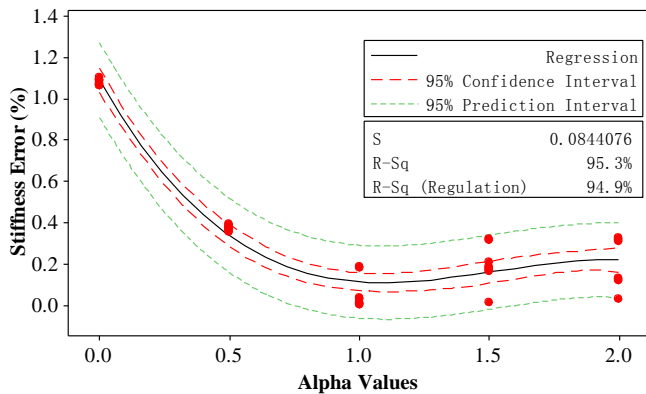


**Fig. 3.** Relationship between the  $\alpha$  Value and Stiffness Error in the DEM Model.

**Table 1.** Values of Input Parameters in the BBR Test Simulation.

Input Parameters	Values
A	0, 0.5, 1, 1.5 and 2
Stiffness E in the DEM Model	Random Stiffness ( $1.0 \times 10^8$ Pa - $9.0 \times 10^8$ Pa)
R (Ball Radius) in the DEM Model	$2.5 \times 10^{-4}$ m
L (Length) in the DEM Model	0.102 m
b (Width) in the DEM Model	$1.25 \times 10^{-2}$ m
h (Height) in the DEM Model	$6.25 \times 10^{-3}$ m
P (Stress) in the DEM Model	0.98 N
L in The Parallel Bond	$5 \times 10^{-4}$ m
$\bar{\lambda}$ in the Parallel Bond	$2.5 \times 10^{-4}$ m

point. Simultaneously, both normal or shear forces and moments at the contact can be transferred through parallel bonds. However, contact bonds can only transmit forces acting at the contact point. Also, a parallel bond can be envisioned as a set of elastic springs with the constant normal stiffness and shear stiffness. These bonds are like two series of parallel springs acting at the contact bond of particles [33]. Thus, the stiffness can be divided following Eq. (1), and the assumption can be described as Eq. (2). Based on Eqs. (1) and (2), Eq. (3) of the stiffness distribution is obtained.

$$E = E_c + E_p \tag{1}$$

$$E_p = \alpha E_c \tag{2}$$

$$E_c = \frac{E}{1 + \alpha}; E_p = \frac{\alpha E}{1 + \alpha} \tag{3}$$

where:

$E$  = random stiffness (Pa)

$E_c$  = contact bond modulus (Pa)

$E_p$  = parallel bond modulus (Pa)

$\alpha$  = coefficient of stiffness distribution

If the two particles have the same normal stiffness and shear stiffness, then the moduli of contact bond and parallel bond [33] are shown as follow:

Contact bond modulus:

$$K_n = K_s = 2Ec \begin{cases} t & (PFC^{2D}) \\ 2R & (PFC^{3D}) \end{cases} \tag{4}$$

Parallel bond modulus:

$$K^n = \frac{Ec}{L}; K^s = \frac{Ec}{L} \begin{cases} \varphi^2, (PFC^{2D}) \\ \frac{3\varphi^2}{4}, (PFC^{3D}) \end{cases} \quad \text{with } \varphi = \frac{\bar{R}}{\tilde{R}} \tag{5}$$

$$\bar{R} = \bar{\lambda} \min(R^{[A]}, R^{[B]}) \tag{6}$$

$$\bar{\lambda} = R; L = 2R \tag{7}$$

where:

$R^{[A]}, R^{[B]}$  = two closed ball radiuses in the DEM model (m)

$L$  = thickness parameter in the parallel bond (m)

$\bar{\lambda}$  = parallel bond radius (m)

For the DEM model, Eq. (7) was used for parallel bond parameters. Simultaneously, five  $\alpha$  values were chosen: 0, 0.5, 1, 1.5 and 2. At the beginning, 15 randomly appointed values for the stiffness of elastic model were selected arbitrarily, and the range is between  $1.0 \times 10^8$  Pa and  $9.0 \times 10^8$  Pa. Then, the parameters of the contact bond and parallel bond were adopted, and the time independent BBR test simulation was conducted. From the deflection records of beam in the BBR test simulation, the stiffness at the specific time were calculated using Eq. (14). At the same time, the stiffness between the input and output were compared, and the stiffness errors and input parameters are shown in Fig. 3 and Table 1.

Fig. 3 indicates that if the value of  $\alpha$  is 1.0941, the minimum value of the stiffness error can be found. Therefore, the relationship between contact bond and parallel bond is obtained, and the coefficient of  $\alpha$  is determined.

### Validation of Discrete Element Model

It is well-known that the three-point beam has a unique characteristic. No matter what the material property is and when the constant load is applied to the three-point beam, the horizontal stress is not changed. Only the beam model's dimension and loading can influence the stress. In this DEM simulation, the theoretical stress equation of the beam middle is shown in Eq. (8), and the equation of error between the theory result and simulation result is shown in Eq. (9). In order to validate the discrete element model, a time-independent discrete element simulation was performed, and the stress of the beam middle is shown in Fig. 4.

$$\text{Theory Stress } \sigma_{11} = \frac{3Pl}{2bh^2} \tag{8}$$

$$\text{Relative Error} = \frac{\text{Theory stress} - \text{Simulation stress}}{\text{Theory Stress}} \times 100\% \tag{9}$$

where:

$P$  = constant load (N)

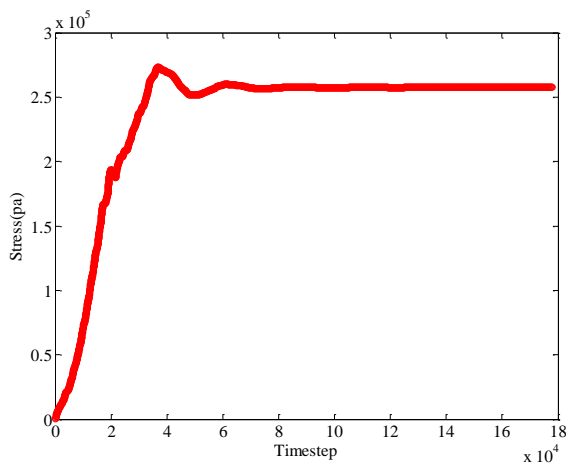


Fig. 4. Stress of the X-axis in the DEM Simulation Model.

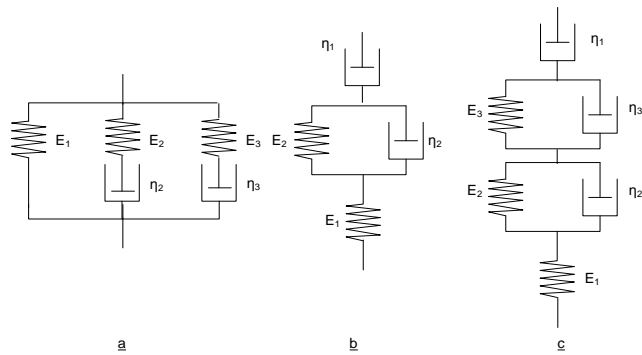


Fig. 5. (a) Generalized Maxwell Model (Five Elements); (b) Burger Model (Four Elements); (c) Generalized Kelvin Model (Six Elements).

$l$  = length of BBR model (m)  
 $b$  = width of BBR model (m)  
 $h$  = height of BBR model (m)

Fig. 4 shows that the steady stress of the x-axis is  $2.6 \times 10^5$  Pa, and the stress of the theoretical solution is  $2.8 \times 10^5$  Pa from Eq. (8). Therefore, based on Eq. (9), the error between the theoretical stress and simulation stress is 7.1%. It is an acceptable result [34] due to the relatively small model size and thickness approximation.

### Experimental Tests and Data Analysis

The asphalt BBR test represents the low temperature performance of asphalt binder. It is necessary to find a viscoelastic model to describe the stiffness trend in the data analysis. Afterwards, the Generalized Maxwell model, Generalized Kelvin model, and Burger model were used to fit the BBR test results.

The Generalized Maxwell model is well-known as the Maxwell-Wiechert model. It expresses the behavior of linear viscoelasticity and considers the relaxation as a distribution of time. The model includes many spring-dashpot Maxwell elements. Based on the accuracy requirement of the model, the number of spring and dashpot can be changed [35, 36]. The model is shown in Fig. 5(a), and the relaxation modulus equations are shown in Eqs. (10) and (11).

$$E(t) = \{E_e\} + \sum_{n=1}^{\infty} E_n \exp\left(-\frac{t}{\tau_n}\right) \quad (10)$$

$$\tau_n = \eta/E_n \quad (11)$$

The Maxwell model and Kelvin model are the basic models to describe the performance of viscoelastic materials. Burger's model is composed of the Maxwell model and the Kelvin model, which are connected in a series. Also, it usually represents the creep behavior of the viscoelastic materials [17]. The model equation and figure are shown in Eq. (12) and Fig. 5(b).

$$\varepsilon(t) = \sigma_0 \left[ \frac{1}{E_1} + \frac{t}{\eta_1} + \frac{1}{E_2} \left( 1 - e^{-\frac{\eta_2}{E_2} t} \right) \right] \quad (12)$$

The Generalized Kelvin model is the extensions or generalizations of the 3- and 4- parameter Voigt models [35]. The model equation and figure are shown in Eq. (13) and Fig. 5(c).

$$\varepsilon(t) = \sigma_0 \left[ \frac{1}{E_1} + \frac{t}{\eta_1} + \sum_2^n \frac{1}{E_2} \left( 1 - e^{-\frac{\eta_2}{E_2} t} \right) \right] \quad (13)$$

where:

- $E(t)$  = stiffness modulus of the Generalized Maxwell model (Pa)
- $E_e$  = stiffness modulus of the extra spring in the Generalized Maxwell model (Pa)
- $E_n$  = stiffness modulus of the spring in the Generalized Maxwell model (Pa)
- $\eta_n$  = dashpot viscosity in the Generalized Maxwell model (Pa.s)
- $E_1$  = stiffness modulus of spring 1 (Pa)
- $E_2$  = stiffness modulus of spring 2 (Pa)
- $\eta_1$  = dashpot 1 viscosity (Pa.s)
- $\eta_2$  = dashpot 2 viscosity (Pa.s)
- $\tau_n$  = relaxation time (s)
- $\varepsilon(t)$  = model strain
- $\sigma_0$  = model stress (N)

The micro-carbon, nanotube material was selected and considered as the asphalt binder modifier. The nano-modified asphalt was prepared using the high shear machine. According to the Superpave™ Specification, the BBR test should be conducted at  $-24^\circ\text{C}$  temperature [17]. The calculation equation of BBR test stiffness is shown in Eq. (14), and the model parameters are shown in Table 2.

$$S(t) = \frac{Pl^3}{4bh^3\delta(t)} \quad (14)$$

where:

- $P$  = constant load of BBR sample (N)
- $l$  = length of BBR sample (m)
- $b$  = width of BBR sample (m)
- $h$  = height of BBR sample (m)
- $S(t)$  = asphalt binder stiffness modulus at a specific time
- $\delta(t)$  = deflection at a specific time

**Table 2.** Parameters of All Models.

Model	Parameters
Burger’s Model (Four Elements: Two Spring and Two Dashpot)	$E_1= 396.9 \text{ Pa}$
	$E_2= 10,443.8 \text{ Pa}$
	$\eta_1= 2,839.1 \text{ Pa}\cdot\text{s}$
	$\eta_2= 20,348.6 \text{ Pa}\cdot\text{s}$
Generalized Maxwell Model (Five Elements: Three Spring and Two Dashpot)	$E_1= 179.8 \text{ Pa}$
	$E_2= 256.8 \text{ Pa}$
	$E_3= 505.2 \text{ Pa}$
	$\eta_2= 5,166.8 \text{ Pa}\cdot\text{s}$
	$\eta_3= 1,000.0 \text{ Pa}\cdot\text{s}$
Generalized Kelvin Model (n=3 and Six Elements: Three Spring and Three Dashpot)	$E_1= 250,000.0 \text{ Pa}$
	$E_2= 700.8 \text{ Pa}\cdot\text{s}$
	$E_3= 844.0 \text{ Pa}$
	$\eta_1= 20,353.5 \text{ Pa}\cdot\text{s}$
	$\eta_2= 25,000.0 \text{ Pa}\cdot\text{s}$
	$\eta_3= 25,000.0 \text{ Pa}\cdot\text{s}$

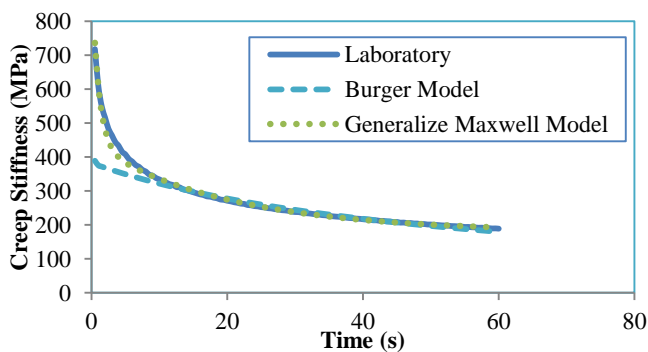


**Fig.6.** Generalized Maxwell Model, Burger’s Model and Laboratory Test Results.

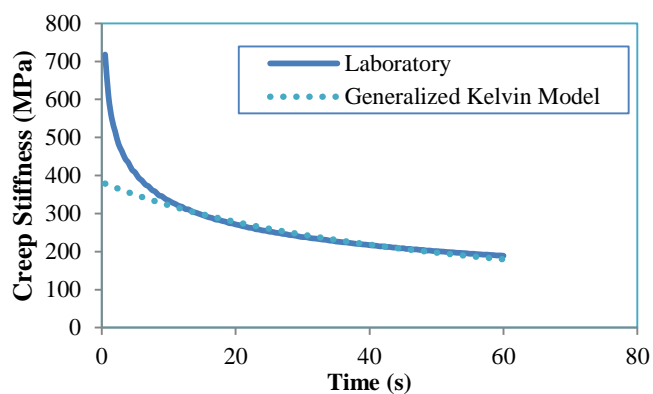


**Fig. 7.** Generalized Kelvin Model and Laboratory Test Results.

Figs. 6 and 7 demonstrate the comparison between the laboratory results and mathematical models. The Generalized Maxwell model results are similar with the laboratory results, and the Generalized Kelvin model and Burger model results are close to the laboratory results after 10 second. The behavior of asphalt at low temperatures is not purely viscoelastic when loading is applied. However, from the constitution of these two models (generalized Kelvin model and Burger’s model), they are suitable for the viscoelastic material simulation. This most likely results in the difference between the simulation and laboratory data. Meanwhile, from the constitution of

the Generalized Maxwell model, the spring in the parallel position of the model holds the elastic property of the model. However, the parallel Maxwell models in the Generalized Maxwell model show viscoelastic property. That potentially corresponds to the similar results between simulation and laboratory data.

### Time-dependent Discrete Element Simulation of BBR Test

In this discrete element simulation, the input moduli were found from Eqs. (10) to (13), and model parameters are shown in Table 2. Then, the moduli of contact bond and parallel bond were distributed by Eqs. (6) and (7). The continuous inputs,  $E_c$  and  $E_p$ , were obtained, and the 0.98 N load was applied. Within each time period, the time-dependent relaxation modulus of asphalt was assumed to be constant. In the simulation, the time-step of the discrete element simulation was less than  $10^{-7}$  second. Therefore, the parameters of the model and material were prepared, and the process of BBR testing was simulated. The deflections of the bending beam were gained, and the contact bond force and displacement of simulation model are shown in Figs. 8 and 9. Also, the comparison results between the laboratory data and simulation data (Generalized Maxwell model) of control and nano-modified asphalt binders were conducted. The data are shown from Figs. 10 to 12.

In Fig. 8, the tension stress of the beam model was concentrated to the bottom of the beam’s middle. However, the compressive stress of the beam model was concentrated to the top of the beam’s middle. In Fig. 9, the displacement tendency of the bending beam is shown, and the beam middle has the largest displacement compared to other positions of the bending beam. Fig. 10 reveals that the beam middle deflections between the simulation and laboratory results of control and nano-modified asphalt binders are very close to each other. Also, in Fig. 11, a similar tendency happens in the stiffness results between the simulation and laboratory data of control and nano-modified asphalt binders. Moreover, Fig. 12 shows that the R-squared values of the DEM simulation (Generalized Maxwell model) of control and nano-modified asphalt binders are 0.99, which means that the stiffness results between the simulation and laboratory data are very similar. As shown in Table 3, different modeling results of the control and nano-modified asphalt binders were compared in terms of the R-square value and the root mean square error (RMSE). It was found that the generalized Maxwell model is a promising approach for fitting the BBR testing data. Therefore, as long as the test time-domain is discretized and the



**Fig.8.** Contact Force of DEM Model in the BBR Test Simulation.



**Fig. 9.** Displacement of DEM Model in The BBR Test Simulation.

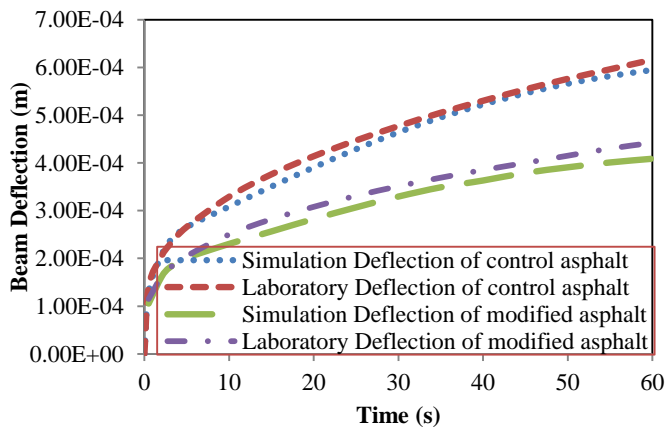


**Fig. 10.** Deflection Comparison between the Simulation and Laboratory Data of Control and Nano-modified Asphalt Binders (Generalized Maxwell Model).

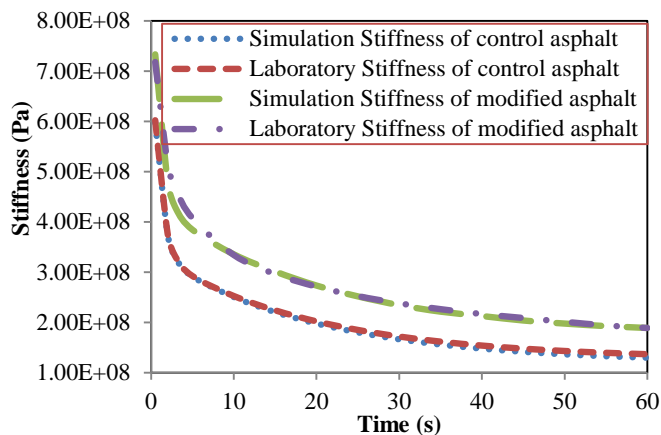


**Fig. 11.** Stiffness Comparison between the Simulation and Laboratory Data of Control and Nano-modified Asphalt Binders (Generalized Maxwell Model).

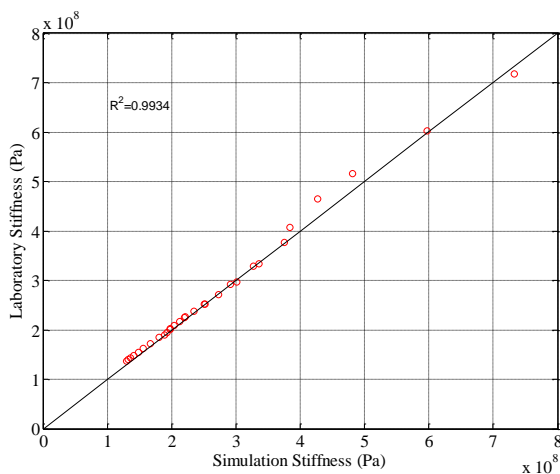


**Fig. 12.** R-squared Value between the Simulation Stiffness and Laboratory Stiffness of Control and Nano-modified Asphalt Binders (Generalized Maxwell Model).

**Table 3.** Models' Comparison Results of R-Squared Value and Root Mean Square Error (RMSE).

Model	R <sup>2</sup>	Root Mean Square Error (RMSE)
Burger's Model (modified asphalt, four Elements: two spring elements and two dashpot elements)	0.82	98.10
Generalized Maxwell Model (modified asphalt, five elements: three spring elements and two dashpot elements)	0.99	15.32
Generalized Kelvin Model (modified asphalt, n=3 and six elements: three spring elements and three dashpot elements)	0.80	100.38
Burger's Model (control asphalt, four elements: two spring elements and two dashpot elements)	0.75	264.31
Generalized Maxwell Model (control asphalt, five elements: three spring elements and two dashpot elements)	0.99	4.95
Generalized Kelvin Model (control asphalt, n=3 and six elements: three spring elements and three dashpot elements)	0.74	264.31

continuous modulus is inputted, the BBR test can be simulated using the linear elastic model of discrete element.

### Summary and Conclusions

In order to improve the understanding of control and nanomaterial modified asphalt, this paper presents a numerical simulation with a three-dimensional discrete element model for BBR tests of control and nanomaterial modified asphalt. Laboratory tests of BBR and data analysis methods were introduced to capture model inputs and validate the simulation results. The following conclusions are brief summaries about the findings observed from this research:

1. The relationship between contact bond and parallel bond was brought out in the simulation model, and the parameters of the model were determined. These research findings can be applied to other modeling applications; for instance, in the simulation of concrete materials. Combining the contact bond and parallel bond in the discrete element model, the time-dependent BBR test of modified asphalt binder can be simulated by discretizing the time-domain and inputting continuous modulus with the linear elastic model. In addition, smaller errors between the laboratory test and simulation results were shown.
2. From the R-squared values and root mean square error (RMSE) results, the Generalized Maxwell model is more suitable for fitting BBR test data under low temperatures compared to Burger's model and the Generalized model.

3. In the bending beam, the compressive stress is concentrated on the top of the beam's middle, and tension stress appeared on the bottom of the beam's middle. The fatigue of asphalt binder came out of the bottom of the beam's middle. These simulation results are in accordance with the corresponding theoretical solutions. It indicates the effectiveness of the DEM model.
4. The addition of micro-carbon nanotube material into the control asphalt (PG 64-28) slightly decreased the deflection of asphalt and increased the stiffness in the BBR test. That suggests that the added nanomaterial may not enhance the low temperature of asphalt binder. However, from the Superpave™ Specification, the stiffness values of control and nano-modified asphalt binders at 60 seconds are less than 300MPa, so the corresponding PG grades are identical. This demonstrates that the low temperature of nano-modified asphalt binder did not decrease much.

In summary, the BBR test of asphalt binder can be simulated by DEM using the Generalized Maxwell model. Furthermore, the research focuses on applying the DEM method to simulate the Superpave shear tester (SST) and Asphalt pavement analyzer (APA) tests of asphalt mixtures.

## Acknowledgements

This paper is based in part on work supported by the United States National Science Foundation under Grant CMMI 0701264 and by funds from the National Natural Science Foundation of China under project No. 51178056. Additionally, the material is supported by the Special Fund for Basic Scientific Research of Central Colleges at Chang'an University under project No. CHD2011JC16. Any opinions, findings, conclusions and recommendations expressed in this paper are those of the authors and do not necessarily reflect the views of participating organizations.

## References

1. Goh, S.W. and Z. You. (2009). Preliminary Study of Evaluating Asphalt Pavement Rutting Performance Using the Mechanistic-Empirical Pavement Design Guide, *ASCE Proceedings of the 14th Conference on Cold Regions Engineering*, pp. 366-373, Duluth, MN, USA.
2. Liu, Y., Dai, Q., and You, Z. (2009). Viscoelastic Model for Discrete Element Simulation of Asphalt Mixtures, *Journal of Engineering Mechanics*, 135(4), pp. 324-333.
3. Liu, Y. and You, Z. (2009). Visualization and Simulation of Asphalt Concrete with Randomly Generated Three-Dimensional Models, *Journal of Computing in Civil Engineering*, 23(6), pp. 340-347.
4. You, Z., Liu, Y., and Dai, Q. (2011). Three-Dimensional Microstructural-based Discrete Element Viscoelastic Modeling of Creep Compliance Tests for Asphalt Mixtures, *Journal of Materials in Civil Engineering*, 23(1), pp. 79-87.
5. You, Z. et al. (2011). Nanoclay-modified Asphalt Materials: Preparation and Characterization, *Construction and Building Materials*, 25(2), pp. 1072-1078.
6. Goh, S.W. et al. (2011). Effect of Deicing Solutions on the Tensile Strength of Micro- or Nano-modified Asphalt Mixture, *Construction and Building Materials*, 25(1), pp. 195-200.
7. Dai, Q. and You, Z. (2007). Prediction of Creep Stiffness of Asphalt Mixture with Micromechanical Finite-Element and Discrete-Element Models, *Journal of Engineering Mechanics*, 133(2), pp. 163-173.
8. You, Z. and Goh, S.W. (2008). Laboratory Evaluation of Warm Mix Asphalt: A Preliminary Study, *International Journal of Pavement Research and Technology*, 1(1), pp. 34-40.
9. Palit, S.K., Reddy, K.S., and Pandey, B.B. (2004). Laboratory Evaluation of Crumb Rubber Modified Asphalt Mixes, *Journal of Materials in Civil Engineering*, 16(1), pp. 45-53.
10. Attaelmanan, M., Feng, C.P., and Ai, A.-H. (2011). Laboratory Evaluation of HMA with High Density Polyethylene As a Modifier. *Construction and Building Materials*, 25(5), pp. 2764-2770.
11. Lundstrom, R. and Isacson, U. (2004). Linear Viscoelastic and Fatigue Characteristics of Styrene-Butadiene-Styrene Modified Asphalt Mixtures. *Journal of Materials in Civil Engineering*, 16(6), pp. 629-638.
12. Zarei, H.R. and Kröger, M. (2008). Bending Behavior of Empty and Foam-filled Beams: Structural Optimization, *International Journal of Impact Engineering*, 35(6), pp. 521-529.
13. Tasdemir, Y. (2009). High Temperature Properties of Wax Modified Binders and Asphalt Mixtures, *Construction and Building Materials*, 23(10), pp. 3220-3224.
14. Peters, S. et al. (2011). Nanocellulose and Microcellulose Fibers for Concrete, *Transportation Research Record*, No. 2142, pp. 25-28.
15. ASTM-D6648 (2008). *Standard Test Method for Determining the Flexural Creep Stiffness of Asphalt Binder Using the Bending Beam Rheometer (BBR)*, American Society for Testing and Materials, West Conshohocken, PA, USA.
16. Takallou, H. et al. (1997). Use of Superpave Technology for Design and Construction of Rubberized Asphalt Mixtures, *Transportation Research Record*, No. 1583, pp. 71-81.
17. Liu, S. et al. (2010). Analysis and Application of Relationships between Low-temperature Rheological Performance Parameters of Asphalt Binders, *Construction and Building Materials*, 24(4), pp. 471-478.
18. Zare-Shahabadi, A., Shokuhfar, A., and Ebrahimi-Nejad, S. (2011). Preparation and Rheological Characterization of Asphalt Binders Reinforced with Layered Silicate Nanoparticles, *Construction and Building Materials*, 24(7), pp. 1239-1244.
19. Lu, X. and Redelius, P. (2007). Effect of Bitumen Wax on Asphalt Mixture Performance, *Construction and Building Materials*, 21(11), pp. 1961-1970.
20. Edwards, Y., Tasdemir, Y., and Isacson, U. (2006). Effects of Commercial Waxes on Asphalt Concrete Mixtures Performance at Low and Medium Temperatures, *Cold Regions Science and Technology*, 45(1), pp. 31-41.
21. Mansoori, G.A. (1997). Modeling of Asphaltene and Other Heavy Organic Depositions, *Journal of Petroleum Science and Engineering*, 17(1-2), pp. 101-111.
22. Shang, L. et al. (2011). Pyrolyzed Wax from Recycled Cross-linked Polyethylene As Warm Mix Asphalt (WMA)

- Additive for SBS Modified Asphalt, *Construction and Building Materials*, 25(2), pp. 886-891.
23. Qian, Z. et al. (2011). Performance Evaluation of a Lightweight Epoxy Asphalt Mixture for Bascule Bridge Pavements, *Construction and Building Materials*, 25(7), pp. 3117-3122.
  24. Ghile, D.B. (2006). Effects of Nanoclay Modification on Rheology of Bitumen and on Performance of Asphalt Mixtures, *Master's Thesis*, Delft University of Technology, Delft, The Netherlands.
  25. Jahromi, S.G. and Khodaii, A. (2009). Effects of Nanoclay on Rheological Properties of Bitumen Binder. *Construction and Building Materials*, 23(8), pp. 2894-2904.
  26. Jahromi, S.G., Andalibizade, B., and Vossough, S. (2009). Engineering Properties of Nanoclay Modified Asphalt Concrete Mixtures, *The Arabian Journal for Science and Engineering*, 35(1B), pp. 89-103.
  27. Pastor, M.M. and F. Roure. (2009). Open Cross-section Beams under Pure Bending II: Finite Element Simulation, *Thin-Walled Structures*, 47(5), pp. 514-521.
  28. Palmer, D.W., Bank, L.C., and Gentry, T.R. (1998). Progressive Tearing Failure of Pultruded Composite Box Beams: Experiment and Simulation, *Composites Science and Technology*, 58(8), pp. 1353-1359.
  29. Liu, Y. and You, Z. (2011). Discrete-Element Modeling: Impacts of Aggregate Sphericity, Orientation, and Angularity on Creep Stiffness of Idealized Asphalt Mixtures, *Journal of Engineering Mechanics*, 137(4), pp. 294-303.
  30. Liu, Y. and You, Z. (2008). Simulation of Cyclic Loading Tests for Asphalt Mixtures Using User Defined Models within Discrete Element Method, *ASCE Proceedings of Sessions of GeoCongress*, pp. 742-749, New Orleans, LA, USA.
  31. Zelelew, H. and Papagiannakis, T. (2010). Simulation of Asphalt Concrete Uniaxial Creep Using Discrete Element Method (DEM), *ASCE Proceedings of Pavements and Materials: Characterization and Modeling Symposium at EMI*, pp. 99-110, Los Angeles, CA, USA.
  32. Liu, Y., You, Z., and Dai, Q. (2011). Stiffness of Sand Mastic versus Stiffness of Asphalt Binder Using Three-Dimensional Discrete Element Method, *ASCE Proceedings of Pavements and Materials: Characterization and Modeling Symposium at EMI*, pp. 54-65, Los Angeles, CA, USA.
  33. Itasca Consulting Group, (2008). *PFC 3D Version 4.0*, Minneapolis, Minnesota, USA.
  34. Liu, Y. (2011). Accelerated Discrete-Element Modeling of Asphalt-Based Materials with the Frequency-Temperature Superposition Principle, *Journal of Engineering Mechanics*, 137(5), p. 355-366.
  35. Tschoegl, N.W. (1989). The Phenomenological Theory of Linear Viscoelastic Behavior, *Springer-Verlag*, Berlin, Germany.
  36. Dai, Q. and You, Z. (2010). A Microstructure-Based Approach for Simulating Viscoelastic Behaviors of Asphalt Mixtures, *ASCE Proceedings of the 2010 GeoShanghai International Conference: Paving Materials and Pavement Analysis (GSP 203)*, pp. 150-161, Shanghai, China.